

## Microstructural evolution and mechanical properties of new multi-phase NiAl-based alloy during heat treatments

XIE Yi(谢 亿)<sup>1,2</sup>, GUO Jian-ting(郭建亭)<sup>2</sup>, ZHOU Lan-zhang(周兰章)<sup>2</sup>,  
CHEN Hong-dong(陈红冬)<sup>1</sup>, LONG Yi(龙 毅)<sup>1</sup>

1. Hunan Electric Power Test and Research Institute, Changsha 410007, China;  
2. Institute of Metal Research, Chinese Academy of Sciences, Shenyang 110016, China

Received 26 November 2009; accepted 4 April 2010

**Abstract:** Microstructural evolution and the relationship between microstructure and property during heat treatments in a new NiAl-based alloy (Ni-26.6Al-13.4Cr-8.1Co-4.3Ti-1.3W-0.9Mo, molar fraction, %) were investigated. The as-cast alloy is composed of NiAl matrix and Cr<sub>3</sub>Ni<sub>2</sub> phase with poor ductility. The Cr<sub>3</sub>Ni<sub>2</sub> phase is distributed as a network along the NiAl grain boundaries. Subsequent heat treatment (1 523 K, 20 h, air cooling+1 123 K, 16 h, furnace cooling) leads to the dissolution of Cr<sub>3</sub>Ni<sub>2</sub> phase and the precipitation of lath-shaped Ni<sub>3</sub>Al phase and  $\alpha$ -Cr particles, resulting in the improvement of compressive properties and fracture toughness at room temperature. Followed by long-term thermal exposure (1 173 K, 8 500 h), it is found that the residual Cr<sub>3</sub>Ni<sub>2</sub> phase keeps stable while the  $\alpha$ -Cr particles coarsen and a great mass of lath-shaped Ni<sub>3</sub>Al precipitates are degenerated, which compromises most of the above improvements of mechanical properties through heat treatment.

**Key words:** NiAl-based alloy; heat treatment; microstructure; mechanical properties

### 1 Introduction

Nickel aluminides based on NiAl exhibit considerable potential for near-term application in various branches of modern industry due to lots of advantages, such as low density, high melting temperature, high thermal conductivity and high specific modulus. Nickel aluminides based on NiAl exhibit considerable potential for near-term application in various branches of modern industry due to lots of advantages, such as low density, high melting temperature, high thermal conductivity, high specific modulus and excellent environmental resistances[1–3]. However, ductility and fracture toughness of these alloys at room and intermediate temperatures are still lower than the desired values for production implementation.

To improve the mechanical properties of NiAl, much work has been done during the past thirty years. CUI et al[4–6] had added Hf element to directionally solidified NiAl-Cr(Mo) near eutectic alloy and developed a series of high-temperature strength alloys,

while the Hf addition decreased the ductility evidently at the same time. NiAl-based composites with Al<sub>2</sub>O<sub>3</sub> fibers were reinforced by complicated process[7–9]. Although the research about process and microstructure at the interface between NiAl and fibers attracted much attention, the mechanical properties have not been reported up to now. For other common methods such as grain refinement, the improved NiAl-based alloy could not meet the criterion of production implementation.

Ni<sub>3</sub>Al and  $\alpha$ -Cr phases could toughen NiAl-based alloy[10–14]. Compared with the single NiAl phase, NiAl matrix of the multiphase compounds have more mobile dislocations slipping from ductile phases[15–17]. In addition, Ti and W were effective strengthening elements for NiAl alloy[10, 18–21]. In this work, a new multi-phase alloy (Ni-26.6Al-13.4Cr-8.1Co-4.3Ti-1.3W-0.9Mo, molar fraction, %) including ductile phases and strengthening elements is fabricated through macro-alloying. Subsequent heat treatments are carried out to modify its microstructure. microstructures are identified. The influences of heat treatments on microstructure and mechanical properties are also discussed.

## 2 Experimental

Master alloy of the experimental material was prepared by induction melting of superalloy K444 and aluminum blocks. Table 1 lists the nominal compositions of the as-cast alloy. The specimens were cut by electron discharge machining (EDM) from the ingot and then heat treated under the schedule of (1 523 K, 20 h, air cooling)+(1 123 K, 16 h, furnace cooling). Parts of the heat-treated specimens were long-term aged at 1 173 K for 8 500 h.

**Table 1** Nominal composition of as-cast alloy (molar fraction, %)

Al	Cr	Co	Ti	W
26.6	13.4	8.1	4.3	1.3
Mo	C	B	Ni	
0.9	0.3	0.3	Bal.	

Microstructure was analyzed using scanning electron microscope (SEM) and transmission electron microscope (TEM). SEM, coupled with energy dispersive X-ray spectroscopy (EDX), was performed with 20 kV accelerating voltage using a JEOL JSM-6301F field emission gun (FEG) scanning electron microscope. Each datum presented in the report is an average of 3 readings by FEG-SEM-EDAX attachment. TEM analysis was conducted using a JEOL 2000 FX II TEM operating at 200 kV. SEM samples were prepared using 25 mL HCl + 2.5 mL H<sub>2</sub>SO<sub>4</sub> + 10 g CuSO<sub>4</sub> + 100 mL H<sub>2</sub>O as etchant. Samples for TEM were thinned mechanically to a thickness of about 50 μm and then ion milled to the final thickness.

Compression specimens with dimensions of 4 mm×4 mm×6 mm were taken by electron discharge machining. All the incisal surfaces were ground to 1 000 grit by abrasive paper. The compressive testing was conducted in air with a Gleeble-1500 testing machine at room temperature under the initial strain rate of  $1.94 \times 10^{-3} \text{ s}^{-1}$ . The autographically recorded load—time curves were converted to true stress—strain curves by taking constant volume into account.

Fracture toughness of the alloy at room temperature was measured by the three-point bending method. Specimens with dimensions of 5 mm×10 mm×50 mm were cut by electron discharge machining. A fatigue pre-crack was not introduced at the notch tip. Prior to the toughness testing, all incisal layers were ground to a finish of 1 000 grit. Then the specimens were loaded in

flexure over a 40 mm span on a MTS880 machine. The crosshead speed was 18 mm/h.

## 3 Results and discussion

### 3.1 Microstructural evolutions

Fig.1 shows the microstructure of the as-cast alloy, which is composed of a white phase (Ni-31.63Al-7.20Cr-6.03Co-3.24Ti-0.32W, molar fraction, %) and NiAl matrix phase (Cr-17.19Co-18.55Ni-6.37Mo-6.97W, molar fraction, %). The Cr-rich phase distributed along the NiAl matrix grain boundaries is further identified as Cr<sub>3</sub>Ni<sub>2</sub> compound through TEM (see Fig.2). Cr<sub>3</sub>Ni<sub>2</sub> compound is demonstrated to be a brittle phase in Ref.[22].

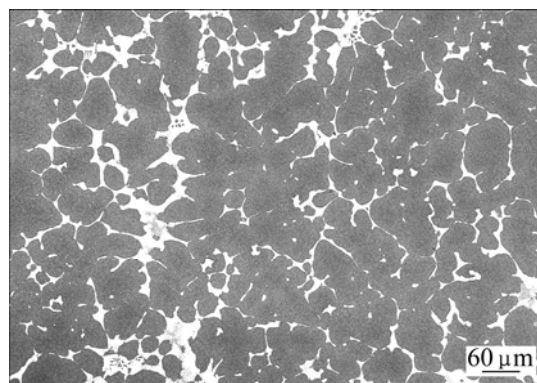


**Fig.1** SEM BSE (back scattered electron) micrograph of as-cast alloy

Microstructure of the alloy after heat treatment of (1 523 K, 20 h, air cooling)+(1 123 K, 16 h, furnace cooling) is shown in Fig.3. Compared with the as-cast alloy, there are three differences in this heat-treated alloy: 1) Cr<sub>3</sub>Ni<sub>2</sub> phase is still distributed along the grain boundaries of NiAl matrix, but becomes small and discontinuous; 2) there exist lath-shaped precipitates in the NiAl matrix; 3) close observation in Fig.3(b) shows that substantive small spherical particles are precipitated from the NiAl matrix. Fig.4 shows the TEM micrograph of the lath-shaped and spherical precipitates which are identified as Ni<sub>3</sub>Al and α-Cr phases respectively by their corresponding diffraction patterns.

During the solution treatment at 1 523 K, the Cr<sub>3</sub>Ni<sub>2</sub> phase dissolved, and the Cr and Ni atoms from the dissolved Cr<sub>3</sub>Ni<sub>2</sub> phase diffused into the NiAl matrix[22]. Due to the fast cooling rate (AC), no precipitates formed after cooling.

Subsequent short aging at 1 123 K (1 123 K, 16 h, furnace cooling) results in the precipitation of Ni<sub>3</sub>Al and α-Cr phase from the saturated NiAl matrix rich in Cr and

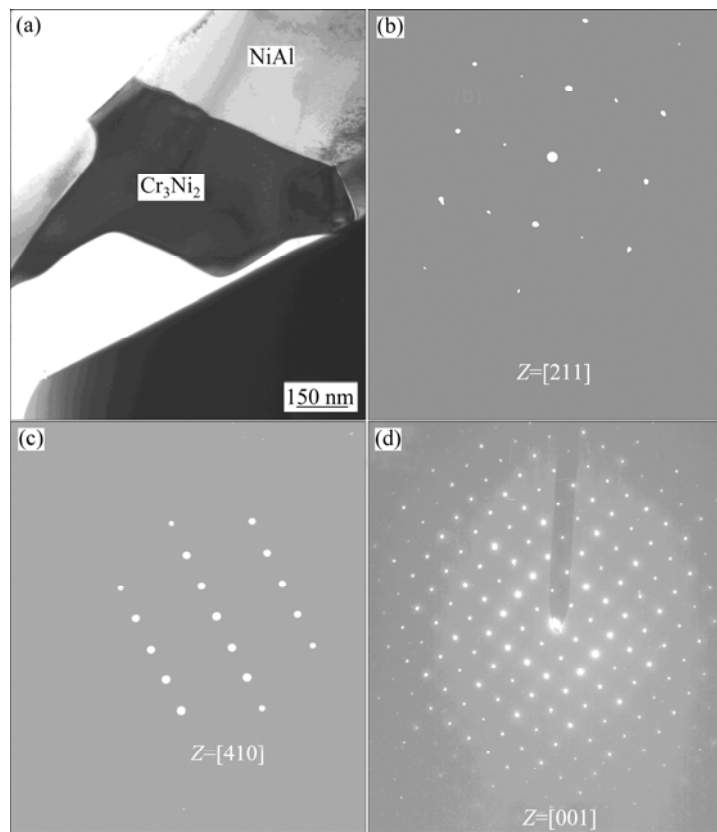


**Fig.2** Bright field TEM image (a) of NiAl and Cr<sub>3</sub>Ni<sub>2</sub> phases in as-cast alloy and their corresponding diffraction patterns of NiAl along zone axis [211] (b) and Cr<sub>3</sub>Ni<sub>2</sub> along zone axes [410] (c) and [001] (d)

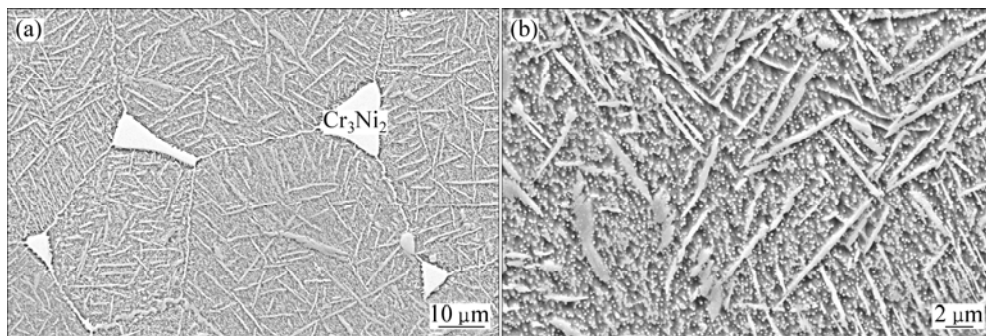


**Fig.3** SEM second electron micrographs of alloy after heat treatment

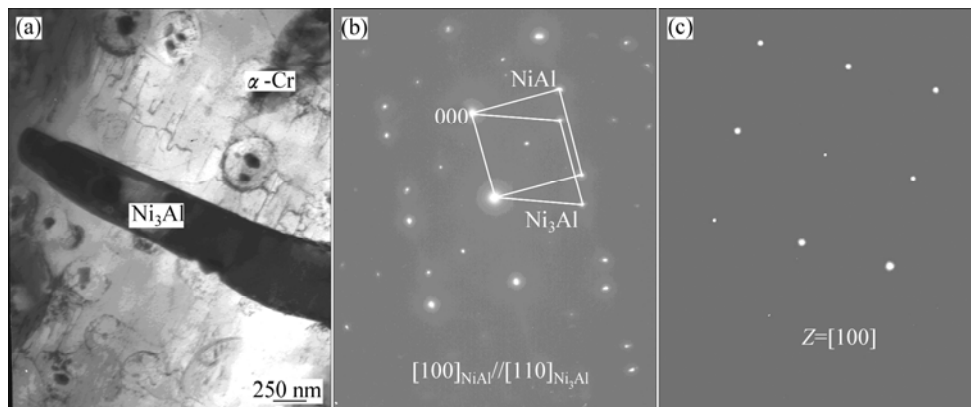
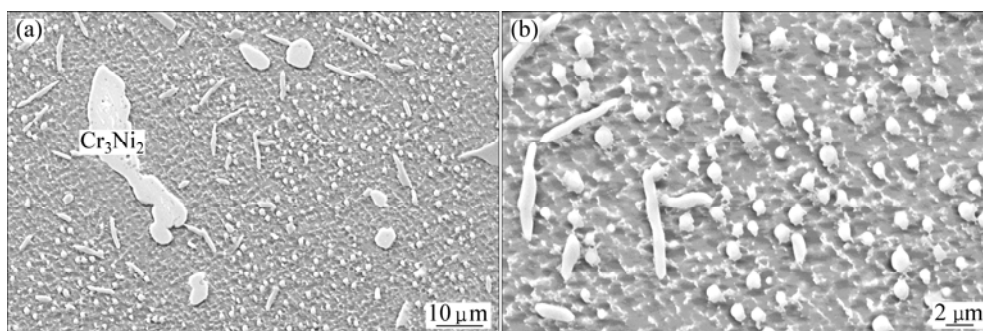


**Fig.4** Bright field TEM image (a) of Ni<sub>3</sub>Al and α-Cr precipitates in alloy after heat treatment and their corresponding diffraction patterns of Ni<sub>3</sub>Al along zone axis [110] (b), α-Cr along zone axis [100] (c)

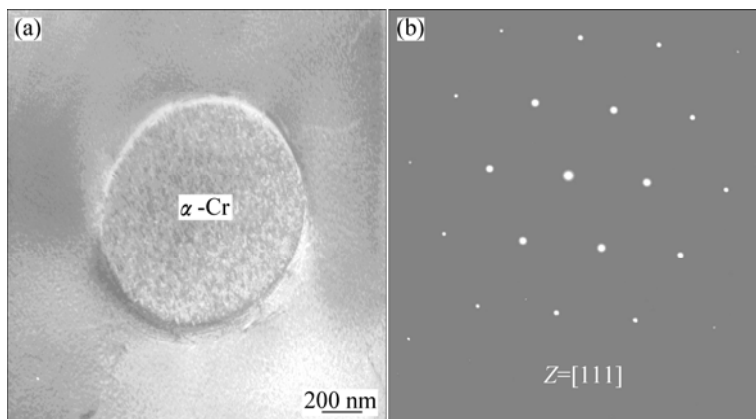
Ni element. EDS reveals that the composition of NiAl matrix in the as-cast alloy is Ni-31.63Al-7.20Cr-6.03Co-3.24Ti-0.32W, as seen in Table 2. According to the NiAl binary phase diagram and NiAl-Cr pseudo-binary phase diagram[23–24],  $\text{Ni}_3\text{Al}$  and  $\alpha\text{-Cr}$  should be precipitated in NiAl alloy containing Al ranging from 27% to 41% and NiAlCr alloy with more than 7% Cr (molar fraction), respectively, after aging treatment of (1 123 K, 16 h, furnace cooling). The experimental results in this work are in good agreement with the phase diagrams.

Fig.5 shows the microstructure of the alloy after long-term aging at 1 173 K for 8 500 h. Except the NiAl

matrix and the discontinuous  $\text{Cr}_3\text{Ni}_2$  phase, short rod-shaped and spherical precipitates are found in this heat treated alloy. SAD patterns in Fig.6 and Fig.7 indicate that the short rod-shaped precipitates are  $\text{Ni}_3\text{Al}$  phase and the spherical particles are  $\alpha\text{-Cr}$  phase. The size and morphology of the two kinds of precipitates in Fig.5 are different from those in Fig.3. This means that the long-term aging (1 173 K, 8 500 h) leads to the coarsening of  $\alpha\text{-Cr}$  particles and the degeneration of lath-shaped  $\text{Ni}_3\text{Al}$  precipitates. LAPIN and VANO[25] also observed the coarsening phenomenon of  $\alpha\text{-Cr}$  particles in the Ni-Al-Cr-Ti type alloy with the additions



**Fig.5** SEM second electron micrographs of alloy after long-term aging



**Fig.6** Bright field TEM image (a) of  $\alpha\text{-Cr}$  precipitate in alloy after long-term aging and corresponding diffraction pattern along zone axis [111] (b)

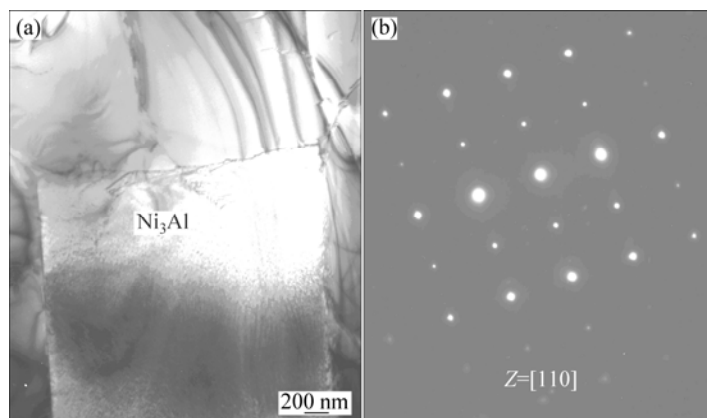


**Fig.7** Bright field TEM image (a) of  $\text{Ni}_3\text{Al}$  precipitate in alloy after long-term aging and corresponding diffraction pattern along zone axis [110] (b)

of Mo and Zr during heat treatment.

### 3.2 Mechanical Properties

Fig.8 shows the room temperature compression behavior for the present alloys. For comparison, the curve of the NiAl-28Cr-6Mo-0.05Sc[26] eutectic alloy is also plotted. The result indicates that the present alloy after heat treatment obtains the combination of improved compressive strength up to more than 1800 MPa and good compressive ductility which is comparable with that of NiAl-28Cr-6Mo-0.05Sc alloy (see Fig.8). Compared with this heat treatment state, the alloys at the as-cast and long-term aging states show lower strength and almost no plastic ductility.

It is known that the microstructure influences the mechanical properties. Network-shaped brittle  $\text{Cr}_3\text{Ni}_2$  phase may cause catastrophic damage. It is confirmed that there is smooth cleavage in the continuous  $\text{Cr}_3\text{Ni}_2$  phase on the fracture surface after the three-point bending test, as seen in Fig.9. On the other hands, the  $\text{Ni}_3\text{Al}$  precipitates embedded in NiAl matrix can enhance the room temperature compressive plasticity and impact

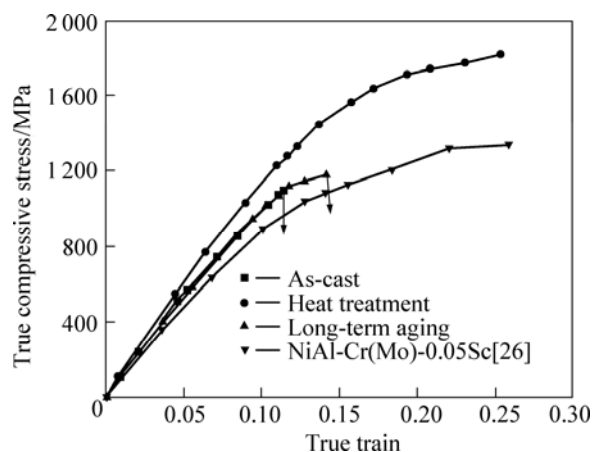


**Fig.8** True stress—true strain curves of present alloy under different states and NiAl-Cr(Mo)-0.05Sc[26] eutectic alloy tested at room temperature (“→” indicates onset of crack growth)

resistance[27]. MISRA et al[28] found that the directional solidified Ni-30Al exhibits up to 9% of tensile ductility at room temperature due to the addition

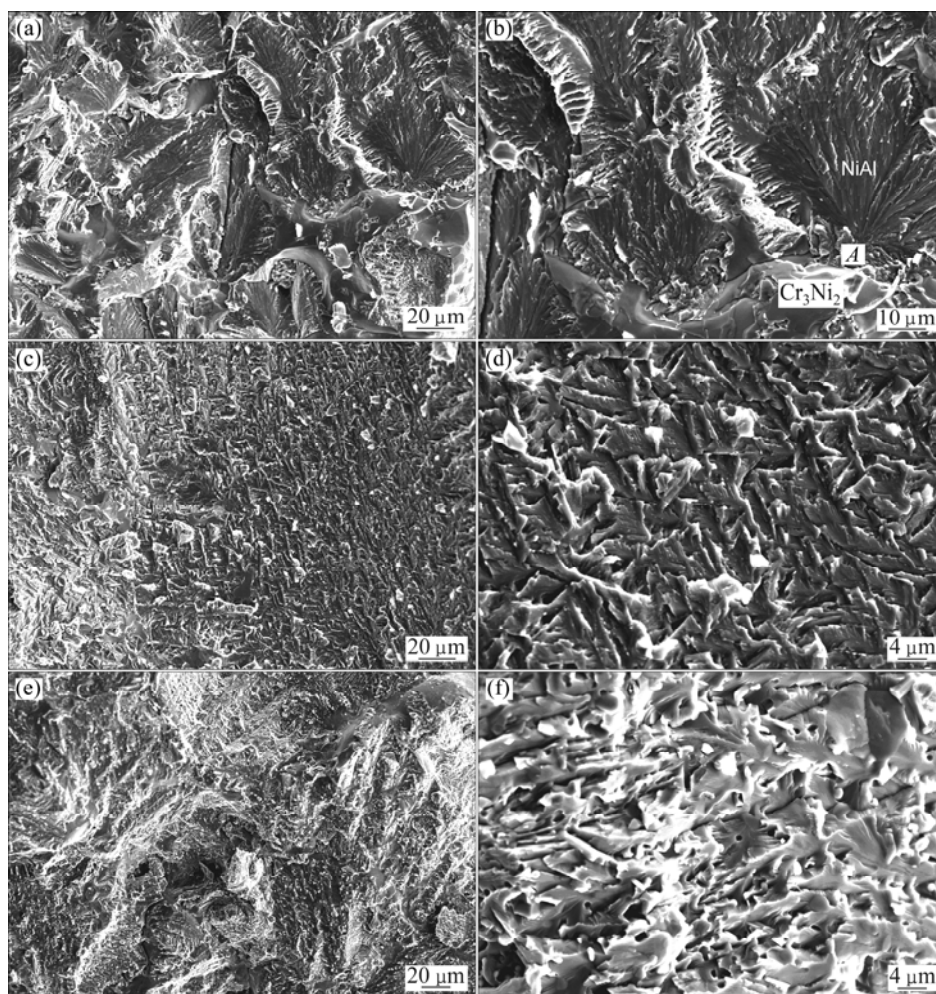


**Fig.9** SEM second electron images of fracture surface of alloys after three-point bending test at room temperature: (a)–(b) As-cast alloy; (c)–(d) Heat treated alloy; (e)–(f) Long-term aged alloy (A in Fig.9(b) represents source of crack initiation.)

of Ni<sub>3</sub>Al phase. The present alloy after heat treatment acquired an optimum microstructure. The brittle Cr<sub>3</sub>Ni<sub>2</sub> distributed continuously along the NiAl matrix grain boundaries was dissolved in this heat treatment. In addition, ductile lath-shaped Ni<sub>3</sub>Al phase and  $\alpha$ -Cr particles were precipitated. This marked change in microstructure gives rise to the improvement of the compressive properties.

The fracture toughness,  $K_Q$  values of the present alloy under different states are summarized in Table 2. Among these three states, the heat treated alloy possesses the highest fracture toughness value of 8.6 MPa·m<sup>1/2</sup>. The mechanisms of fracture in the present alloy were characterized by SEM fractography, as shown in Fig.9. The predominant model of fracture in the as-cast alloy was intergranular fracture. The network-shaped Cr<sub>3</sub>Ni<sub>2</sub> phase failed in cleavage and became the fracture initiation point (Fig.9(b)). The cleavage fracture propagated into the NiAl matrix in a radiant direction. Because of the microstructural evolution, fracture model changed after heat treatment. Big cleavage facets disappeared. Lath-shaped Ni<sub>3</sub>Al precipitates blunted the crack tips and obstructed the fracture paths. In this case, the  $K_Q$  value was enhanced. The fracture toughness of the alloy after long-term aging is 7.4 MPa·m<sup>1/2</sup>, better than that of the as-cast alloy but worse than that of the heat-treated alloy. When the crack propagated in the alloy after long-term aging, the  $\alpha$ -Cr particles coarsened during the long-term aging and deflected and obstructed the fracture paths instead of Ni<sub>3</sub>Al precipitates. However, the attribution of the  $\alpha$ -Cr particles to the fracture resistance is less than that of Ni<sub>3</sub>Al precipitates in the heat-treated alloy.

**Table 2** Mechanical properties of present alloy under different states

State	Compressive strength/MPa	Compressive strain/%	Fracture toughness/(MPa·m <sup>1/2</sup> )
As-cast	1095	0.0	6.3
Heat treatment	1815	10.5	8.6
Long-term aging	1180	2.5	7.4

## 4 Conclusions

1) The as-cast alloy (Ni-26.6Al-13.4Cr-8.1Co-4.3Ti-1.3W-0.9Mo, molar fraction, %) is composed of NiAl and Cr<sub>3</sub>Ni<sub>2</sub> phases which are distributed along the NiAl matrix grain boundaries as a network. During heat treatment, the Cr<sub>3</sub>Ni<sub>2</sub> phase dissolves and becomes discontinuous; lath-shaped Ni<sub>3</sub>Al and small spherical

$\alpha$ -Cr particles are precipitated from the NiAl matrix. Then the long-term aging exposure results in the coarsening of  $\alpha$ -Cr particles and the dissolution of the Ni<sub>3</sub>Al precipitates.

2) The alloy after heat treatment possesses the perfect combination of compressive properties and fracture toughness at room temperature due to the dissolution of brittle Cr<sub>3</sub>Ni<sub>2</sub> phase network and the precipitation of ductile Ni<sub>3</sub>Al and  $\alpha$ -Cr phase. The worsening of the mechanical properties in the alloy after long-term aging is mainly ascribed to the dissolution of Ni<sub>3</sub>Al precipitates.

## References

- [1] NOEBE R D, BOWMAN R R, NATHAL N V. Physics and mechanical properties of the B2 compound NiAl [J]. Int Mater Rev, 1993, 38(44): 193–232.
- [2] MIRACLE D B. The physical and mechanical properties of NiAl [J]. Acta Metall Mater, 1993, 41(3): 649–684.
- [3] BHANU K, RAO S, RAJ B. Advances in the development of creep and fatigue resistance materials [J]. Metallurgical and Materials Engineering, 2003, 28: 695–708.
- [4] CUI C Y, CHEN Y X, GUO J T, LI D X, YE H Q. Preliminary investigation of directionally solidified NiAl-28Cr-5.5Mo-0.5Hf composite [J]. Mater Lett, 2000, 43(1/2): 303–308.
- [5] CUI C Y, GUO J T, YE H Q. Effects of Hf additions on high-temperature mechanical properties of a directionally solidified NiAl/Cr(Mo) eutectic alloy [J]. Journal of Alloys and Compounds, 2008, 463(2): 263–270.
- [6] GUO J T, CUI C Y, CHEN Y X, LI D X, YE H Q. Microstructure, interface and mechanical property of the DS NiAl/Cr(Mo,Hf) composite [J]. Intermetallics, 2001, 9(4): 287–297.
- [7] LIU C, JENG S M, YANG J M, AMATO R A. Processing and high temperature deformation of Al<sub>2</sub>O<sub>3</sub> fiber-reinforced NiAlFe matrix composites [J]. Mater Sci Eng A, 1995, 191: 49–59.
- [8] BOWAN R R, MISRA A K, ARNOLSD S M. Processing and mechanical properties of Al<sub>2</sub>O<sub>3</sub> fiber-reinforced NiAl composites [J]. Metall Mater Trans A, 1995, 26: 615–628.
- [9] DAVID E H, STEPAN K, JOCHEN M S. Effect of a BN interlayer on the tensile strength of NiAl coated sapphire fibers [J]. Scripta Mater, 2006, 55: 219–222.
- [10] LAPIN J, PELACHOVA T, BAJANA O. Microstructure and mechanical properties of a directionally solidified and aged intermetallic Ni-Al-Cr-Ti alloy with  $\beta$ - $\gamma'$ - $\gamma$ - $\alpha$  structure [J]. Intermetallics, 2000, 8(12): 1417–1427.
- [11] MORRIS J R, YE Y Y, LEEY B, HARMON B N, GSCHNRIDNER J K, RUSSELL A M. Ab initio calculation of bulk and defect properties of ductile rare-earth intermetallic compounds [J]. Acta Mater, 2004, 52: 4849–4857.
- [12] ZEUMER B, SAUTHOFF G. Deformation behavior of intermetallic NiAl-Ta alloys with strengthening Laves phase for high-temperature applications III: Effects of alloying with Cr [J]. Intermetallics, 1998, 6: 451–460.
- [13] JOHNSON D R, OLIVER B F, NOEBE R D, WHITTENBERGER J D. NiAl-based polyphase in situ composites in the NiAl-Ta-X(X=Cr, Mo, V) systems [J]. Intermetallics, 1995, 3: 493–503
- [14] TIAN W H, HAN C S, NEMOTO M. Precipitation of  $\alpha$ -Cr in B2-ordered NiAl [J]. Intermetallics, 1999, 7: 59–67.

- [15] NORBE R D, MISRA A, GIBALA R. Plastic flow and fracture of B2 NiAl-based intermetallic alloys containing a ductile second phase [J]. ISIJ International, 1991, 31(10): 1172–1185.
- [16] MISRA A, GIBALA R. Room-temperature deformation behavior of directionally solidified multiphase Ni-Fe-Al alloys [J]. Metall Mater Trans A, 1997, 28: 795–807.
- [17] MISRA A, GIBALA R. Plasticity in multiphase intermetallics [J]. Intermetallics, 2000, 8: 1025–1034.
- [18] LI H T, WANG Q, HE J C, GUO J T.  $\beta$ -Ti(M) solid solution formation and its thermal stability in a NiAl-Cr(Mo)-(Hf,Ti) near eutectic alloy [J]. Materials Characterization, 2007, 59(10): 1395–1399.
- [19] LI H T, GUO J T, YE H Q. Composition dependence of the precipitation behavior in NiAl-Cr(Mo)-(Ti, Hf) near eutectic alloys [J]. Mater Sci Eng A, 2007, 452(15): 763–772.
- [20] LI H T, GUO J T, YE H Q. Simultaneous improvement of strength and ductility in NiAl-Cr(Mo)-Hf near eutectic alloy by small amount of Ti alloying addition [J]. Materials Letters, 2008, 62: 61–64.
- [21] TANG L Z, ZHANG Z G, LI S S, GONG S K. Mechanical behaviors of NiAl-Cr(Mo)-based near eutectic alloy with Ti, Hf, Nb and W additions [J]. Transactions of Nonferrous Metals Society of China, 2010, 20: 212–216.
- [22] XIE Y, ZHOU L Z, GUO J T, YE H Q. Effect of heat treatment on the microstructure of multiphase NiAl-based alloy [J]. J Mater Sci Technol, 2008, 24(2): 245–250.
- [23] MASSALSKI T B, OKAMOTO H, SUBRAMANIAN P R, KALPRZAK L. Binary alloy phase diagrams [M]. Ohio: ASM International, 1990: 183–184.
- [24] VILLARS P, PRINCE A, OKAMOTO H. Handbook of ternary alloy phase diagrams [M]. Ohio: ASM International, 1995: 3161.
- [25] LAPIN J, VANO A. Coarsening kinetics of  $\alpha$ - and  $\gamma'$ -precipitates in a multiphase intermetallic Ni-Al-Cr-Ti type alloy with additions of Mo and Zr [J]. Scripta Mater, 2004, 50(5): 571–575.
- [26] XIE Y, GUO J T, ZHOU L Z, LIANG Y C, YE H Q. Micro-structure and mechanical properties of the alloys NiAl and NiAl-28Cr-6Mo doped with rare-earth Sc [J]. Acta Meta Sini, 2008, 44(5): 529–534.(in Chinese)
- [27] RUSSELL K C, EDINGTON J W. Precipitation behaviour and mechanical properties of a nickel 36at.% aluminium alloy [J]. Met Sci J, 1972, 6: 20–24.
- [28] MISRA A, GIBALA R, NOEBE R D. Deformation and fracture behavior of a directionally solidified beta/gamma Ni-30at.pct Al alloy [J]. Metall Mater Trans A, 1999, 30 (4): 1003–1015.

(Edited by LI Xiang-qun)